Supporting Information

Molecular anchoring-induced proton adsorption effect achieves stable zinc metal anodes

Dajin Liu[a,b*], Bangdi Lv[a], Zihao Liu[a], Lu Cheng[a], Yu Deng[c], Xinchun Song[c], and Zhipeng Jiang[c*]

[a] College of Mechanical Engineering, Tongling University, No.4 Cuihu Road, Tongling 244100, China

[b] Advanced Copper-based Material Industry Generic Technology Research Center of Anhui Province, No.4 Cuihu Road, Tongling 244100, China

[c] School of Materials Science and Engineering, Anhui University of Technology, Maanshan 243002, China

Corresponding E-mail address: gips332@163.com, jzp1994@ahut.edu.cn

1. Experimental

1.1 Material and methods

1.1.1 *Electrolyte preparation*

Zinc sulfate heptahydrate ($ZnSO_4 \cdot 7H_2O$, Aladdin Chemicals, purity >99%) was utilized as the Zn source to prepare aqueous electrolytes. A base solution of 2 M Zn concentration was initially formulated by dissolving the crystalline salt in deionized water. Subsequently, dicyandiamide ($C_2H_4N_4$, Aladdin) was introduced as an additive at varying molar ratios (0.01, 0.02, and 0.05 M) through controlled dissolution in the ZnSO4 electrolyte. The resulting mixtures were designated as ZSO + 0.01 M DCD, ZSO + 0.02 M DCD, and ZSO + 0.05 M DCD respectively. Systematic evaluation revealed that the 0.02 M DCD-modified electrolyte exhibited optimal electrochemical performance under standardized testing conditions.

1.1.2 *Preparation of $NH_4V_4O_{10}$ Cathode Material*

A mixture containing 200 mg of sodium dodecyl benzene sulfonate (SDBS) and 0.005 M of ammonium metavanadate (NH_4VO_3) were dissolved in 60 mL of deionized water (DI) and then stirred continuously for 30 min. After adding 1.5 mL of diluted sulfuric acid and stirring the mixture for another 30 min, the mixture turned orange-yellow. The homogeneous solution was transferred into a hydrothermal autoclave and maintained at 200 °C for a period of 24 h. The resulting green solid, identified as $NH_4V_4O_{10}$, was thoroughly rinsed with ethanol and DI alternately and subsequently dried in an oven at 70 °C.[1]

1.1.3 *Cell preparation*

A homogeneous mixture was prepared by combining $NH_4V_4O_{10}$, Super P (DoDoChem), and polyvinylidene difluoride (PVDF, DoDoChem) in a mass ratio of 7:2:1, which was then dispersed in 1-methyl-2-pyrrolidone (NMP, 99.9%, Innochem). The resulting slurry was evenly applied onto a Ti foil (20 μm thickness). The coated foil was cut into circular cathodes (Φ 8 mm) and a mass loading of 1.3 mg cm^{-2} after drying at 80 °C. For high-loading cathodes, $NH_4V_4O_{10}$, Super P, and polytetrafluoroethylene emulsion (PTFE, Canrd) were mixed in a 7:2:1 ratio and coated onto stainless steel meshs (S = 2.0 cm^2), then dried overnight at 80 °C. The Zn-

$NH_4V_4O_{10}$ cells were constructed using an $NH_4V_4O_{10}$ cathode, a Whatman glass fiber separator (Φ 19 mm, GF/D), and a Zn foil anode (100 μm thickness, Φ 14 mm, 99.99% purity). Notably, for high-loading $NH_4V_4O_{10}$ cathodes, the Zn anode thickness was adjusted to 10 μm. The voltage range in which the cells were cycled was 0.2-1.8 V, and self-discharge performance was evaluated at 1 A g^{-1}. Cu cathodes measuring Φ16 mm and 12 μm in thickness was used for Zn-Cu half-cells. Zn-Cu half-cells, Zn-Zn symmetric cells, and Zn- $NH_4V_4O_{10}$ cells were assembled for cyclic performance evaluation. All cycling tests for CR2032 cells were performed at controlled room temperature (25 ℃) using the Neware battery testing system from Neware Technology Co., Ltd.

1.2 Characterizations

Raman spectral characterization was performed on both electrolytes and post-cycled Zn anodes using a LabRAM HR800 system. Nuclear magnetic resonance (NMR) spectroscopy analysis was conducted on three electrolyte formulations (2 M $ZnSO_4$ in D_2O, 0.02 M DCD in D_2O, and and 2 M $ZnSO_4$ + 0.02 M DCD in D_2O) using Bruker Avance NEO 400 MHz. Surface topography evaluation of cycled Zn anodes was achieved through micron-scale roughness via Bruker Dimension Icon atomic force microscopy and field-emission scanning electron microscopy (Zeiss Sigma 300). Using Thermo Scientific K-Alpha, x-ray photoelectron spectroscopy (XPS) was carried out on the cycled Zn surface. In situ optical monitoring of Zn deposition behavior was implemented through a XPV 800E microscope system coupled with a transparent quartz. Using Nicolet iS20, Thermo Fisher, the Zn anode after cycling was tested by Fourier-transform infrared spectroscopy (FTIR) spectroscopy. The practicality of Zn-$NH_4V_4O_{10}$ cells was validated through practical demonstration using an LED light strip. The crystalline phase identification of the cathode material was performed by X-ray diffraction analysis (XRD) using MiniFlex600 with Cu Kα radiation.

1.3 Electrochemical measurements

Chronoamperometry (CA) measurements were conducted on Zn-Zn symmetric cells by applying a constant overpotential of -150 mV for a duration of 300 s, while Tafel plots were simultaneously generated using the same cells at 5 mV s^{-1}. Linear

sweep voltammetry (LSV) was carried out on Zn-Cu half-cells at 1 mV s^{-1}. With an applied scan rate of 5 mV s^{-1} and over a frequency range of 100 kHz to 0.1 Hz, electrochemical impedance spectroscopy (EIS) was conducted. At 1 mV s^{-1}, cyclic voltammetry (CV) tests were performed.

1.4 Theoretical calculations

The first-principles calculations of adsorption energies were conducted using the Vienna *Ab* Initio Simulation Package (VASP) with projector augmented wave (PAW) pseudo-potentials to describe core-electron interactions.[2, 3] The exchange-correlation effects were treated through the generalized gradient approximation (GGA) employing the Perdew-Burke-Ernzerhof (PBE) functional.[4, 5] A plane-wave cutoff energy of 520 eV was implemented, with convergence thresholds set at 10^{-5} eV for electronic self-consistency and 0.05 eV·$Å^{-1}$ for ionic relaxation. Van der Waals interactions were incorporated through the DFT-D3 dispersion correction method within the Grimme scheme.[6] A vacuum of 15 Å was set to avoid interaction along z-axis of Zn (002). The Brillouin zone was sampled with the Gamma centered Monkhorst-Pack scheme k-point grid of 1×1×1 for geometry optimization.[7]

The computational investigations in this study were conducted through density functional theory (DFT) simulations implemented in the DMol3 computational framework. The exchange-correlation interactions were modeled using the generalized gradient approximation (GGA) approach, with the atomic orbital descriptions of all the constituent elements are realised by means of a double-numerical plus polarization (DNP) basis set.[4, 8] Geometric optimizations were performed under strict convergence thresholds, where energy variations, residual forces, and atomic displacements were respectively constrained to 1×10^{-5} Ha, 0.002 Ha/Å, and 0.005 Å. Transition state characterization employed the LST/QST (linear/quadratic synchronous transit) methodology to rigorously confirm saddle point configurations and quantitatively evaluate activation energy profiles.[9]

2. Supplementary Figures

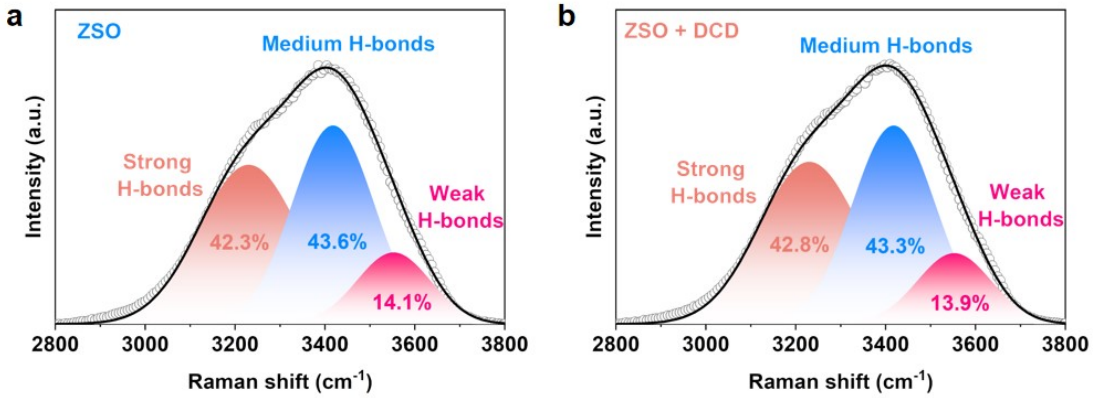

Figure S1 Raman spectra of O-H bonds in different electrolytes.

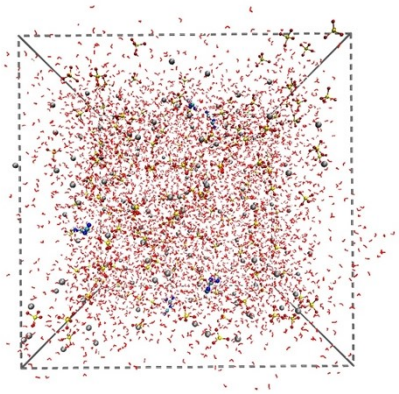

Figure S2 MD simulation snapshot of ZSO+DCD electrolyte.

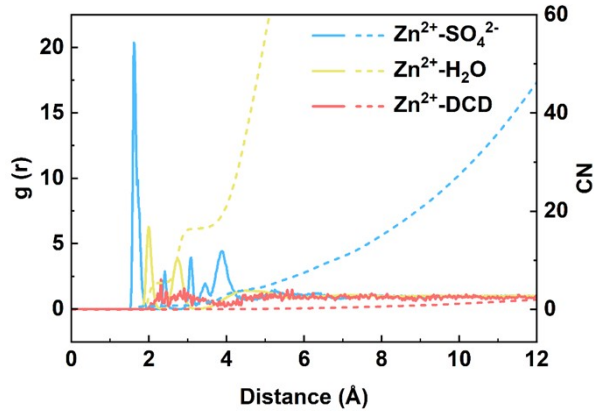

Figure S3 Radial distribution function of ZSO+DCD collected from MD simulation.

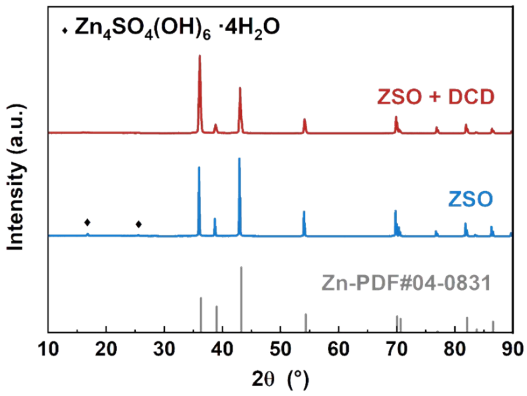

Figure S4 The XRD pattern compared the zinc after 50 hours of cycling in the studied electrolyte with the original zinc under cycling conditions of 1mA cm^{-2} and 1mAh cm^{-2}.

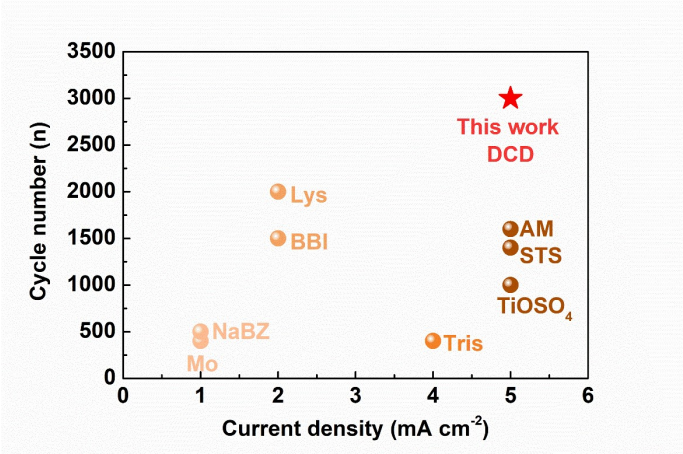

Figure S5. Cycling performance comparisons of Zn-Cu half cells using various electrolyte additives (x mAh cm^{-2}, 1 mAh cm^{-2}). [10-17]

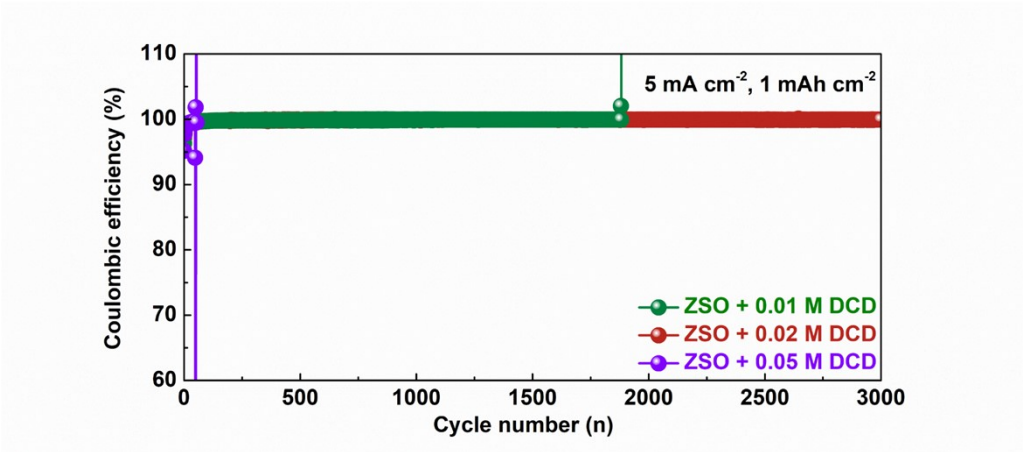

Figure S6. Cycling performance comparison of Zn-Cu half-cells using ZSO electrolytes with different concentrations of DCD (5 mA cm^{-2}, 1 mAh cm^{-2}).

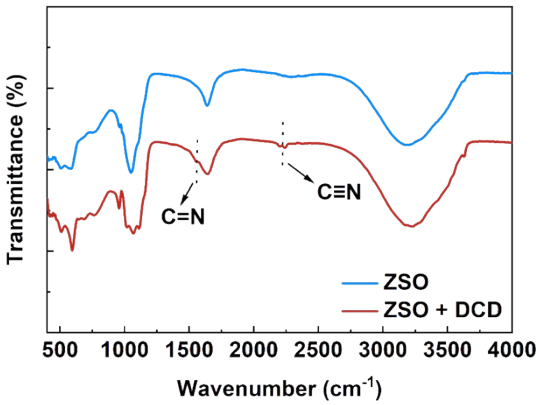

Figure S7. Comparison of FTIR spectra of zinc soaked for 3 days using the studied electrolyte.

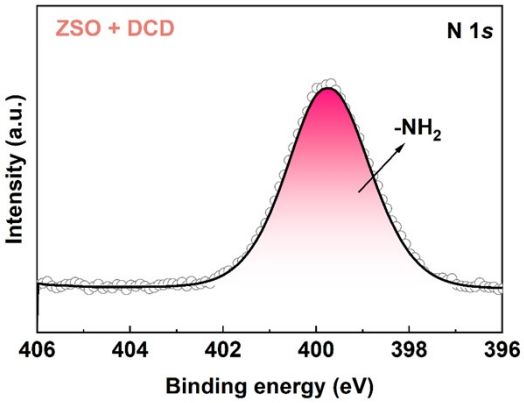

Figure S8. N 1*s* spectra of high-resolution XPS after soaking in ZSO+DCD electrolyte for 3 days.

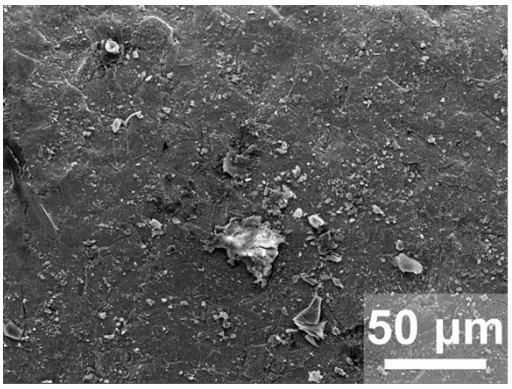

Figure S9. SEM images of cycled Zn anodes using ZSO electrolyte.

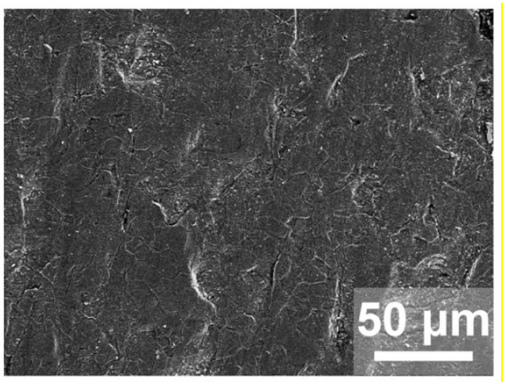

Figure S10. SEM images of cycled Zn anodes using ZSO + DCD electrolyte.

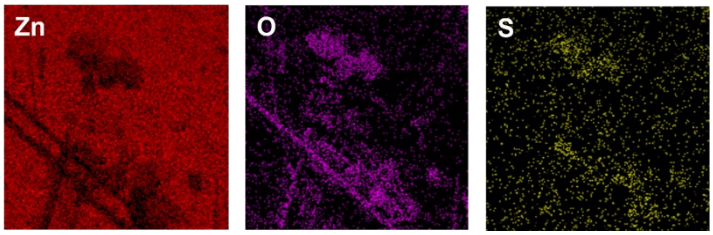

Figure S11. EDS mappings of cycled Zn anodes using ZSO electrolyte.

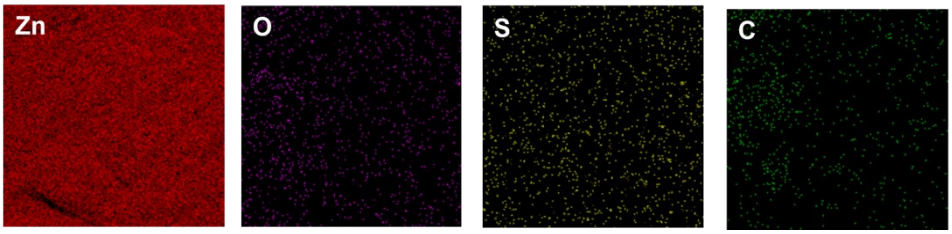

Figure S12. EDS mappings of cycled Zn anodes using ZSO + DCD electrolyte.

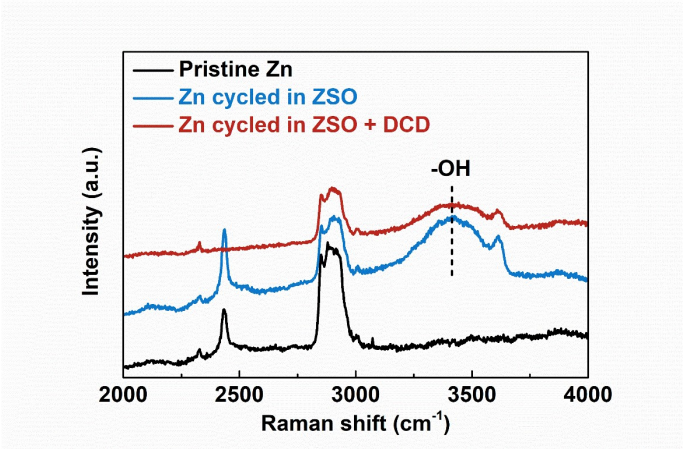

Figure S13. Raman spectra comparison of cycled Zn using the studied electrolyte.

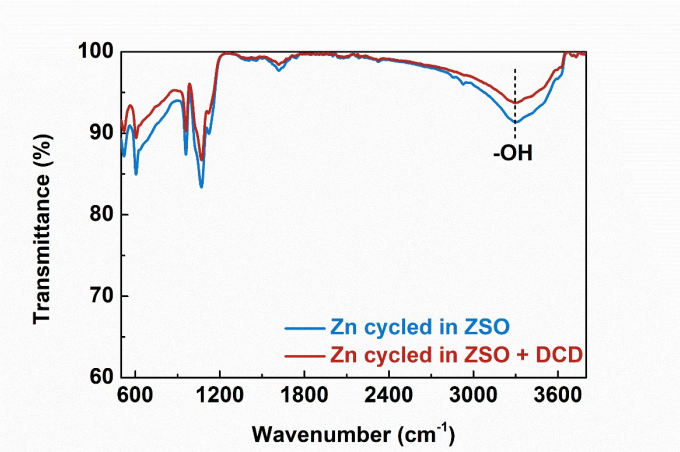

Figure S14. FTIR spectra comparison of cycled Zn using the studied electrolyte.

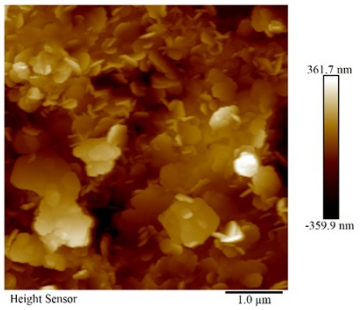

Figure S15. AFM top profile images of cycled Zn anodes using ZSO electrolyte.

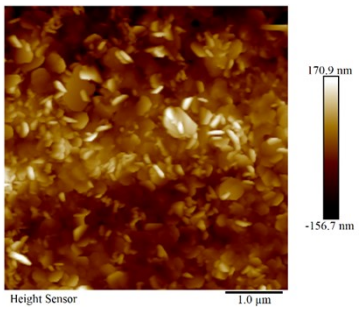

Figure S16. AFM top profile images of cycled Zn anodes using ZSO + DCD electrolyte.

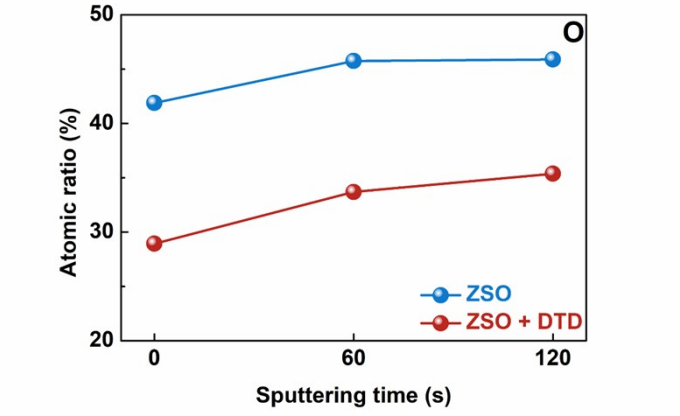

Figure S17. Oxygen content distribution in cycled Zn anodes at varying XPS sputtering depths.

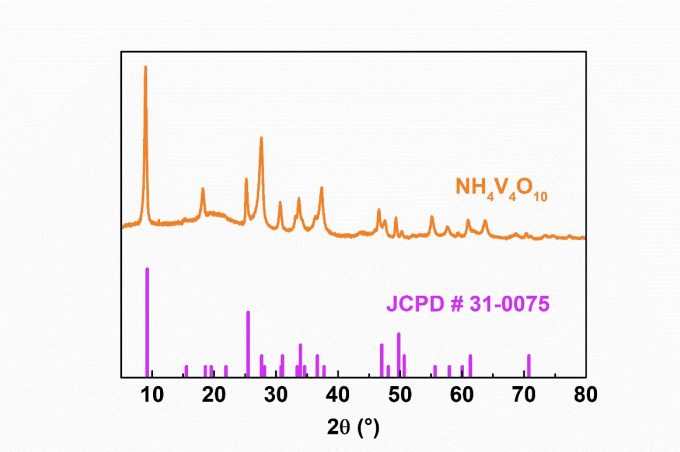

Figure S18. XRD pattern of prepared $NH_4V_4O_{10}$ cathode material.

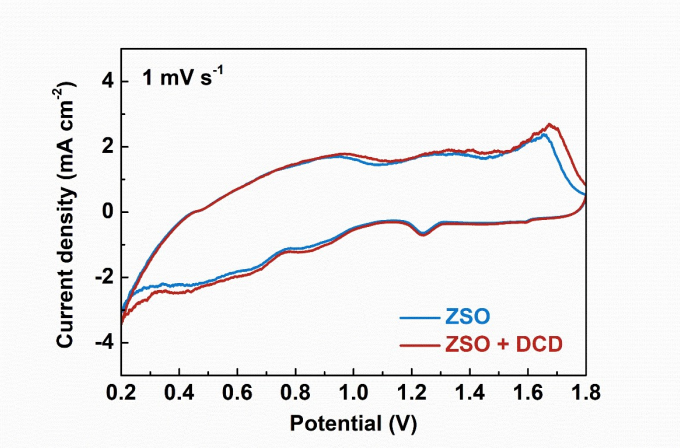

Figure S19. CV curves of Zn-$NH_4V_4O_{10}$ cells with the studied electrolytes.

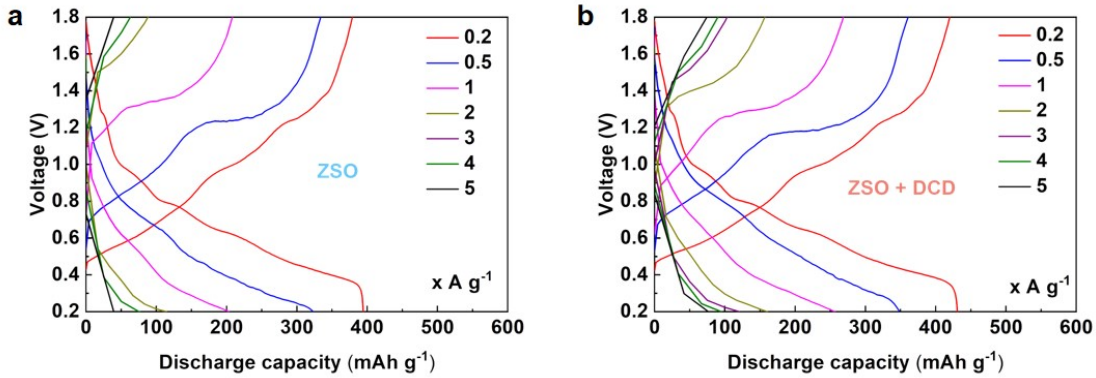

Figure S20. Voltage curves of Zn-$NH_4V_4O_{10}$ cells at different current densities in a) ZSO electrolyte and h) ZSO + DCD electrolyte.

Reference

[1] Y. Peng, L. Mo, T. Wei, Y. Wang, X. Zhang, Z. Li, Y. Huang, G. Yang, L. Hu, *Nano Micro Small* 2024, **20**, 230672.

[2] G. Kresse, J. Furthmüller, *Phys. Rev. B: Condens. Comput. Mater. Sci.* 1996, **6**, 15−50.

[3] G. Kresse, D. Joubert, *Phys. Rev*. B. 1999, **59**, 1758.

[4] J. Perdew, K. Burke, M. Ernzerhof, *Phys. Rev. Lett.* 1996, **77**, 3865.

[5] J. Perdew, M. Ernzerhof, K. Burke, *J. Chem. Phys.* 1996, **105**, 9982−9985.

[6] S. Grimme, J. Antony, S. Ehrlich, H. Krieg, *J. Chem. Phys.* 2010, **132**, 154104.

[7] H. J. Monkhorst, J. D. Pack, *Phys. Rev. B: Solid State* 1976, **13**, 5188.

[8] B. Delley, *J. Chem. Phys.* 2000, **113**, 7756–7764.

[9] A. Tkatchenko, M. Scheffler, *Phys. Rev. Lett.* 2009, **102**, 073005.

[10] H. Liu, Y. Sun, Y. Yang, J. Yang, D. Zhang, R. Chanajaree, X. Wu, X. Zhang, J. Qin, J. Cao, *ACS Appl. Mater. Interfaces* 2024, **16**, 44747-44755.

[11] J. Yu, F. Zhao, J. He, A. Li, C. Que, Z. Chen, L. Tan, Z. Li, Y. Wu, *Chem. Eng. J.* 2024, **487**, 154795.

[12] J. Yin, Y. Luo, M. Li, M. Wu, K. Guo, Z. Wen, *ACS Appl. Mater. Interfaces* 2024, **16**, 53242-53251.

[13] L, Du, Z. Li, W. Song, Q. Bao, P. Wang, Z. Gong, Y. Zhang, Y. Wu, F. Shi, M. Zhou, K. Zhu, *Chem. Eng. J.* 2024, **501**, 157743.

[14] L. N. Aiien, Z. Wang, L. Shan, B. Tang, C. B. Mullins, *ACS Appl. Mater. Interfaces* 2024, **16**, 47599-47609.

[15] Y. Zhou, J. Ma, Y. Yuan, C. Ma, S. Jia, X. Zhang, G. Zhang, X. Zhou, *J. Energy Storage* 2024, **102**, 114123.

[16] J. Zhang, C. Zhou, Y. Xie, Q. Nan, Y. Gao, F. Li, P. Rao, J. Li, X. Tian, X. Shi, *Small* 2024, **20**, 2404237.

[17] Y. Wang, S. Li, L. Li, J. Ren, L. Shen, C. Lai, Tris-buffered efficacy: enhancing stability and reversibility of Zn anode by efficient modulation at Zn/electrolyte interface, *Rare Metals* 2024, **44**, 925−937.